Smart Structures and Systems, *Vol. 24, No. 2 (2019) 209-221*
DOI: https://doi.org/10.12989/sss.2019.24.2.209

An improved Kalman filter for joint estimation of structural states and unknown loadings

Jia He[*1,2], Xiaoxiong Zhang[1,2a] and Naxin Dai[3b]

[1]*College of Civil Engineering, Hunan University, Changsha, China*
[2]*Hunan Provincial Key Lab on Damage Diagnosis for Engineering Structures, Hunan University, Changsha, China*
[3]*The School of Civil Engineering, The University of South China, Hengyang, China*

(Received July 11, 2018, Revised May 10, 2019, Accepted May 13, 2019)

Abstract. The classical Kalman filter (KF) provides a practical and efficient way for state estimation. It is, however, not applicable when the external excitations applied to the structures are unknown. Moreover, it is known the classical KF is only suitable for linear systems and can't handle the nonlinear cases. The aim of this paper is to extend the classical KF approach to circumvent the aforementioned limitations for the joint estimation of structural states and the unknown inputs. On the basis of the scheme of the classical KF, analytical recursive solution of an improved KF approach is derived and presented. A revised form of observation equation is obtained basing on a projection matrix. The structural states and the unknown inputs are then simultaneously estimated with limited measurements in linear or nonlinear systems. The efficiency and accuracy of the proposed approach is verified via a five-story shear building, a simply supported beam, and three sorts of nonlinear hysteretic structures. The shaking table tests of a five-story building structure are also employed for the validation of the robustness of the proposed approach. Numerical and experimental results show that the proposed approach can not only satisfactorily estimate structural states, but also identify unknown loadings with acceptable accuracy for both linear and nonlinear systems.

Keywords: Kalman filter; state estimation; load identification; limited measurements; nonlinear hysteretic structures

1. Introduction

The estimation of the states of a partially observed dynamic system is important for structural health monitoring and vibration control. In this regard, the classical Kalman filter (KF) is a well-recognized recursive algorithm that provides unbiased and optimal state estimation for a linear dynamic system from noise-contaminated response measurements. A variety of KF-based algorithms for state estimation or damage detection have been also studied and well developed. For example, a multi-rate KF approach was proposed by Smyth and Wu (2007) for state estimation when multi-type data with different sampling frequencies were involved. Ching and Beck (2007) presented a novel technique for indirectly monitoring threshold exceedance in a sparsely-instrumented linear structure subject to uncertain excitation modeled as a Gaussian process. A natural state observer, which possessed similar characteristics to the KF in the context of the second order differential equation of motion of linear structural systems, was proposed by Hernandez (2011). The performance of this observer was then investigated via a simulated tall vertical structure subject to turbulent wind load and fatigue damage (Hernandez *et al.* 2013). With the extension use of KF as a damage detector, Bernal (2013) developed a lag shifted whiteness test (LSWT) for damage detection in the presence of changing process and measurement noise. Based on KF algorithm, an integrated method was proposed by Zhu *et al.* (2013) for determining the optimal placement of multi-type sensors and at the same time for reconstructing structural responses at all key locations. He *et al.* (2015) extended this method in the active control system by employing the estimated structural responses for vibration control. Kim and Park (2017) investigated the application of KF for estimating a time-varying process disturbance in a building space.

Although the classical KF and the aforementioned KF-based methods can satisfactorily estimate structural states, the external excitation in these algorithms is assumed to be either known or modeled as a zero mean white Gaussian process. However, in many cases, it is difficult or sometimes impossible to directly measure the input force, or the Gaussian assumption is violated. Therefore, over the past years, various KF with unknown input (KF-UI) methods have been developed to circumvent the above limitations. For example, in the combination of KF and Auto-Regressive-with-eXogenous input (ARX) model, Gao and Lu (2006) proposed a time-domain analysis method for structural damage diagnosis only using acceleration measurements. By making use of unbiased minimum-variance estimation, Gillijns and De Moor (2007a, b) proposed a recursive filter with the structure of KF for the estimation of both unknown inputs and linear system states.

*Corresponding author, Associate Professor
E-mail: jiahe@hnu.edu.cn
[a] Master Student
E-mail: zhangxiaoxiong@163.com
[b] Associate Professor
E-mail: nx.dai@utoronto.ca

ISSN: 1738-1584 (Print), 1738-1991 (Online)

This method was extended by Hsieh (2009) for a general case where not only unknown inputs affected both the system state and the output, but also the direct feedthrough matrix had arbitrary rank. Lourens *et al.* (2012a) also improved this method to cope with the numerical instabilities that arise when the number of sensors surpasses the order of the model. By employing KF to establish a regression model between the residual innovation and the input forces, Wu *et al.* (2009) proposed a method for estimating the time varying excitation force acting on the structural system. Based upon the weighted least-squares estimation and a decomposing method, Pan *et al.* (2011) presented a KF-based input and state estimation method for stochastic linear discrete-time systems with direct feedthrough. By using spectral methods and limited output-only measurements, Papadimitriou *et al.* (2011) proposed a KF-based approach for predicting the strain/stress responses and the associated power spectral densities for fatigue prognosis. Lourens *et al.* (2012b) developed an augmented KF for force identification in structural dynamics, where the unknown inputs were introduced in the state vector and estimated in conjunction with the states. Eftekhar Azam *et al.* (2012a) developed a parallel implementation of the sigma-point Kalman filter (S-PKF) to provide an accurate tracking of the whole state of the laminate. With the comparison of the performances of S-PKF and Particle Filter (PF), Eftekhar Azam *et al.* (2012b) found that the PF displayed a higher convergence rate towards steady-state model calibrations and the S-PKF was less sensitive to the measurement noise. An analytical analysis of the stability of KF-based force estimation techniques was presented by Naets *et al.* (2015), and the addition of dummy measurements on a position level was suggested by the authors to prevent drift. By considering the unknown input as a white process, an output-only KF-based method was presented by Vicario *et al.* (2015) for the estimation of the dynamic structural model solely using time histories of the field measurements. A dual implementation of the KF was conducted by Eftekhar Azam *et al.* (2015a) for estimating the unknown input and states of a linear state-space model. This method was then validated by the authors via a four-story frame structure (Eftekhar Azam *et al.* 2015b). To prevent the so-called drifts in the estimated unknown inputs and structural displacement in the presence of measurement noises, Liu *et al.* (2016) proposed an improved KF with unknown input method basing on data fusion of partial acceleration and displacement measurements. This method was further extended by Lei *et al.* (2016) on the basis of modal KF. More recently, through the implementation of KF under unknown input, Zhang and Xu (2017) presented a novelty damage identification method by utilizing the reconstructed response and excitation. A KF-based inverse approach was developed by Zhi *et al.* (2016, 2017) for the estimation of the wind loads on tall buildings and validated via wind tunnel tests as well as field tests on Taipei 101 Tower. Based on the augmented KF and the modal expansion technique, Ren and Zhou (2017) proposed two strain estimation algorithms for unmeasured members in the truss structure. Based on the synergistic use of proper orthogonal decomposition and KF, Eftekhar Azam *et al.* (2017) proposed an approach for the online health monitoring of damaged structures. By minimizing the overall estimation errors of structural responses at the locations of interest to a desired target level, Hu *et al.* (2018) proposed a KF-based integrated multi-type sensor placement and response reconstruction method for high-rise buildings under unknown seismic loading. Although the KF-UI methods mentioned above can provide promising results of state estimation and loading identification, most of them are suitable to manage linear state-space models. However, nonlinearity exists widely in many civil structures, such as the initiation and growth of damage, the hysteretic characteristics of structural components and so forth.

In this paper, it is aimed to extend the classical KF approach to circumvent the aforementioned limitations for jointly estimating the structural states of linear or nonlinear systems and the unknown inputs applied to them. Based on the scheme of the classical KF, an improved KF-UI approach is proposed and the analytical recursive solutions are derived and given. A revised form of observation equation is obtained with the aid of a projection matrix. The structural states are then estimated with limited measurements. The unknown loadings are identified at the same time by means of least squares estimation. Some numerical examples and shaking table tests on a five-story building structure are used to demonstrate the effectiveness of the proposed approach.

2. Improved KF-UI approach for joint estimation

The equation of motion of an *n* degree-of-freedom (DOF) structure subject to unknown loadings can be given as

$$\mathbf{M}\ddot{\mathbf{x}}(t)+\mathbf{F}[\dot{\mathbf{x}}(t),\mathbf{x}(t),\boldsymbol{\theta}]=\boldsymbol{\varphi}\mathbf{f}(t)+\boldsymbol{\varphi}^{u}\mathbf{f}^{u}(t) \tag{1}$$

where $\ddot{\mathbf{x}}(t),\dot{\mathbf{x}}(t)$ and x(t) are the vectors of structural acceleration, velocity and displacement, respectively; $\mathbf{F}[\dot{\mathbf{x}}(t),\mathbf{x}(t),\boldsymbol{\theta}]$ represents the restoring force vector which can be expressed in the linear or nonlinear form; M is the mass matrix; θ is the structural parameters used to describe the manner of structural restoring force; f(t) and $\mathrm{f}^{u}(t)$ are the known and unknown excitation vectors, respectively; φ and φ^{u} are the influence matrices associated with the known and unknown excitation, respectively.

Define the state vector $\mathbf{Z}(t)=\left[\mathbf{x}(t)^{\mathrm{T}},\dot{\mathbf{x}}(t)^{\mathrm{T}}\right]^{\mathrm{T}}$. Then, a general expression of the state-space equation can be found as

$$\begin{aligned}\dot{\mathbf{Z}}(t)&=\begin{Bmatrix}\dot{\mathbf{x}}(t)\\ \mathbf{M}^{-1}\left[-\mathbf{F}[\dot{\mathbf{x}}(t),\mathbf{x}(t),\boldsymbol{\theta}]+\boldsymbol{\varphi}\mathbf{f}(t)+\boldsymbol{\varphi}^{u}\mathbf{f}^{u}(t)\right]\end{Bmatrix}\\&=\mathbf{g}\left(\mathbf{Z}(t),\mathbf{f}(t),\mathbf{f}^{u}(t),t\right)+\mathbf{w}(t)\end{aligned} \tag{2}$$

where $\mathbf{w}(t)$ is process noise vector with zero mean and a covariance matrix $\mathbf{Q}(t)$.

Let $\hat{\mathbf{Z}}_{k|k}$ and $\hat{\mathbf{f}}_{k}^{u}$ be the estimates of $\mathbf{Z}_{k}$ and $\mathbf{f}_{k}^{u}$ at time $t = k\times\Delta t$ with Δt being time interval, respectively. Eq. (2)

can be then linearized with respect to the estimates $\hat{\mathbf{Z}}_{k|k}$ and $\hat{\mathbf{f}}_k^u$ as follows

$$\mathbf{g}(\mathbf{Z}_k,\mathbf{f}_k,\mathbf{f}_k^u,k\Delta t) \approx \mathbf{g}(\hat{\mathbf{Z}}_{k|k},\mathbf{f}_k,\hat{\mathbf{f}}_k^u,k\Delta t) + \mathbf{U}_{k|k}\left(\mathbf{Z}_k - \hat{\mathbf{Z}}_{k|k}\right) + \mathbf{W}_{k|k}\left(\mathbf{f}_k^u - \hat{\mathbf{f}}_k^u\right) \tag{3}$$

where

$$\mathbf{U}_{k|k} = \left.\frac{\partial \mathbf{g}(\mathbf{Z}_k,\mathbf{f}_k,\mathbf{f}_k^u,k\Delta t)}{\partial \mathbf{Z}_k}\right|_{\mathbf{Z}_k=\hat{\mathbf{Z}}_{k|k},\mathbf{f}_k^u=\hat{\mathbf{f}}_k^u}$$
$$\mathbf{W}_{k|k} = \left.\frac{\partial \mathbf{g}(\mathbf{Z}_k,\mathbf{f}_k,\mathbf{f}_k^u,k\Delta t)}{\partial \mathbf{f}_k^u}\right|_{\mathbf{Z}_k=\hat{\mathbf{Z}}_{k|k},\mathbf{f}_k^u=\hat{\mathbf{f}}_k^u} = \begin{bmatrix}\mathbf{0}\\ \mathbf{M}^{-1}\boldsymbol{\varphi}^u\end{bmatrix} \tag{4}$$

Note $\dot{\mathbf{Z}}(k\Delta t) = (\mathbf{Z}_{k+1} - \mathbf{Z}_k)/\Delta t$, and then the following expression can be derived basing on Eqs. (2)-(4)

$$\mathbf{Z}_{k+1} = \mathbf{Z}_k + \Delta t \cdot [\mathbf{g}(\hat{\mathbf{Z}}_{k|k},\mathbf{f}_k,\hat{\mathbf{f}}_k^u,k\Delta t) + \mathbf{U}_{k|k}\left(\mathbf{Z}_k - \hat{\mathbf{Z}}_{k|k}\right) + \mathbf{W}_{k|k}\left(\mathbf{f}_k^u - \hat{\mathbf{f}}_k^u\right) + \mathbf{w}_k] \tag{5}$$

Usually, the acceleration responses are more reliable and easily obtained, as compared with other structural responses, e.g., displacement or velocity. Moreover, in many practical situations, the structural responses cannot be completely measured due to some factors, such as the cost of the sensors, the inaccessibility of some locations, and the sensor damage subject to the harsh service environments. Therefore, only partial acceleration responses are considered in this study leading to the following discretized observation equation

$$\mathbf{y}_k = \mathbf{L}\ddot{\mathbf{x}}_k + \mathbf{v}_k = \mathbf{L}\mathbf{M}^{-1}\left\{-\mathbf{F}[\dot{\mathbf{x}}_k,\mathbf{x}_k,\boldsymbol{\theta}] + \boldsymbol{\varphi}\mathbf{f}_k + \boldsymbol{\varphi}^u\mathbf{f}_k^u\right\} + \mathbf{v}_k \tag{6}$$

where $\mathbf{y}_k$ is the acceleration measurements at time $t = k\times\Delta t$; $\mathbf{L}$ is the matrix associated with the locations of accelerometers; $\mathbf{F}[\dot{\mathbf{x}}_k,\mathbf{x}_k,\boldsymbol{\theta}]$, $\mathbf{f}_k$ and $\mathbf{f}_k^u$ are the corresponding discretized quantities at time $t = k\times\Delta t$; $\mathbf{v}_k$ is the measurement noise assumed to be a Gaussian white noise with zero mean and a covariance matrix $\mathbf{R}_k$.

Eq. (6) can be also re-arranged as

$$\mathbf{D}\mathbf{f}_k^u = \mathbf{h}(\mathbf{Z}_k) - \mathbf{y}_k + \mathbf{v}_k \tag{7}$$

in which

$$\mathbf{h}(\mathbf{Z}_k) = \mathbf{L}\mathbf{M}^{-1}\left\{-\mathbf{F}[\dot{\mathbf{x}}_k,\mathbf{x}_k,\boldsymbol{\theta}] + \boldsymbol{\varphi}\mathbf{f}_k\right\};\ \mathbf{D} = -\mathbf{L}\mathbf{M}^{-1}\boldsymbol{\varphi}^u \tag{8}$$

Assuming that (i) the number of sensors is larger than that of unknown inputs, and (ii) to ensure matrix $\mathbf{D}$ in Eq. (8) be non-zero the collocated acceleration responses at the location of unknown inputs are measured. Then, the unknown input $\mathbf{f}_k^u$ can be determined by means of least squares estimation as

$$\mathbf{f}_{k,LSE}^u = \left(\mathbf{D}^{\mathrm{T}}\mathbf{D}\right)^{-1}\mathbf{D}^{\mathrm{T}}\left[\mathbf{h}(\mathbf{Z}_k) - \mathbf{y}_k + \mathbf{v}_k\right] \tag{9}$$

The error of the aforementioned solution can be calculated as

$$\begin{aligned}\mathbf{err} &= \mathbf{D}\mathbf{f}_k^u - \mathbf{D}\mathbf{f}_{k,LSE}^u \\ &= \left(\mathbf{I} - \mathbf{D}\left(\mathbf{D}^{\mathrm{T}}\mathbf{D}\right)^{-1}\mathbf{D}^{\mathrm{T}}\right)\left[\mathbf{h}(\mathbf{Z}_k) - \mathbf{y}_k + \mathbf{v}_k\right]\end{aligned} \tag{10}$$

where $\mathbf{I}$ is an identity matrix; $\mathbf{D}\left(\mathbf{D}^{\mathrm{T}}\mathbf{D}\right)^{-1}\mathbf{D}^{\mathrm{T}}$ is known as a projection matrix. As a limit, the error shown in Eq. (10) should tend to be zero, leading to

$$\boldsymbol{\Phi}\mathbf{y}_k = \boldsymbol{\Phi}\mathbf{h}(\mathbf{Z}_k) + \boldsymbol{\Phi}\mathbf{v}_k \tag{11}$$

where $\boldsymbol{\Phi} = \mathbf{I} - \mathbf{D}\left(\mathbf{D}^{\mathrm{T}}\mathbf{D}\right)^{-1}\mathbf{D}^{\mathrm{T}}$. As observed from Eq. (11), with the aid of projection matrix, a revised form of observation equation is obtained. A merit of this observation equation is that the unknown input is not explicitly presented. Thus, the multiple regression problem described by Eq. (6) is transformed into a single regression problem, and then the principle of KF can be employed for the state estimation.

It's known the equations for classical KF falls into two groups: time update equations and measurement update equations. The former is responsible for projecting forward (in time) the current state and error covariance estimates to obtain the a priori estimates for the next time step, whereas the latter is responsible for incorporating a new measurement into the a priori estimate to obtain an improved a posteriori estimate (Welch and Bishop 1995). Since only the linear state-space equation is considered in the classical KF, it is not suitable for nonlinear system. To cover a more general case as mentioned in Eq. (2), the priori state estimate $\hat{\mathbf{Z}}_{k+1|k}$ in this study is calculated as follows

$$\hat{\mathbf{Z}}_{k+1|k} = \hat{\mathbf{Z}}_{k|k} + \int_{k\Delta t}^{(k+1)\Delta t}\mathbf{g}\left(\hat{\mathbf{Z}}_{k|k},\mathbf{f}_k,\hat{\mathbf{f}}_k^u,k\Delta t\right)\mathrm{d}t \tag{12}$$

Taking difference between Eqs. (5) and (12) gives the priori estimate error $\boldsymbol{\varepsilon}_{k+1|k}$ as

$$\boldsymbol{\varepsilon}_{k+1|k} = \left(\mathbf{I} + \Delta t\mathbf{U}_{k|k}\right)\left(\mathbf{Z}_k - \hat{\mathbf{Z}}_{k|k}\right) + \Delta t\mathbf{W}_{k|k}\left(\mathbf{f}_k^u - \hat{\mathbf{f}}_k^u\right) + \Delta t\mathbf{w}_k \tag{13}$$

Based on Eqs. (4), (7) and (8), the second term on the right-hand-side of Eq. (13) can be expressed as

$$\begin{aligned}\Delta t\mathbf{W}_{k|k}(\mathbf{f}_k^u - \hat{\mathbf{f}}_k^u) &= \Delta t\begin{bmatrix}\mathbf{0}\\ \mathbf{M}^{-1}\boldsymbol{\varphi}^u(\mathbf{f}_k^u - \hat{\mathbf{f}}_k^u)\end{bmatrix} \\ &= \Delta t\left\{\begin{matrix}\mathbf{0}\\ -(\mathbf{L}^{\mathrm{T}}\mathbf{L})^{-1}\mathbf{L}^{\mathrm{T}}\left[\mathbf{h}(\mathbf{Z}_k) - \mathbf{h}(\hat{\mathbf{Z}}_{k|k}) + \mathbf{v}_k\right]\end{matrix}\right\}\end{aligned} \tag{14}$$

Similar to Eq. (3), $\mathbf{h}(\mathbf{Z}_k)$ can be linearized with respect to the state estimate $\hat{\mathbf{Z}}_{k|k}$ as follows

$$\mathbf{h}(\mathbf{Z}_k) = \mathbf{h}(\hat{\mathbf{Z}}_{k|k}) + \mathbf{H}_{k|k}\left(\mathbf{Z}_k - \hat{\mathbf{Z}}_{k|k}\right) \tag{15}$$

where

$$\mathbf{H}_{k|k}=\left.\frac{\partial \mathbf{h}(\mathbf{Z}_k)}{\partial \mathbf{Z}_k}\right|_{\mathbf{Z}_k=\hat{\mathbf{Z}}_{k|k}} \tag{16}$$

Then, the priori estimate error $\boldsymbol{\varepsilon}_{k+1|k}$ shown in Eq. (13) can be rewritten as

$$\begin{aligned}\boldsymbol{\varepsilon}_{k+1|k}&=\boldsymbol{\Gamma}_1\left(\mathbf{Z}_k-\hat{\mathbf{Z}}_{k|k}\right)+\boldsymbol{\Gamma}_2\mathbf{v}_k+\Delta t\mathbf{w}_k\\&=\boldsymbol{\Gamma}_1\boldsymbol{\varepsilon}_{k|k}+\boldsymbol{\Gamma}_2\mathbf{v}_k+\Delta t\mathbf{w}_k\end{aligned} \tag{17}$$

where

$$\begin{aligned}\boldsymbol{\Gamma}_1&=\mathbf{I}+\Delta t\mathbf{U}_{k|k}+\Delta t\begin{bmatrix}\mathbf{0}\\-(\mathbf{L}^{\mathrm{T}}\mathbf{L})^{-1}\mathbf{L}^{\mathrm{T}}\mathbf{H}_{k|k}\end{bmatrix};\\\boldsymbol{\Gamma}_2&=\Delta t\begin{bmatrix}\mathbf{0}\\-(\mathbf{L}^{\mathrm{T}}\mathbf{L})^{-1}\mathbf{L}^{\mathrm{T}}\end{bmatrix}\end{aligned} \tag{18}$$

Then, the priori estimate error covariance matrix can be found as

$$\mathbf{P}_{k+1|k}=E\left(\boldsymbol{\varepsilon}_{k+1|k}\boldsymbol{\varepsilon}_{k+1|k}^{\mathrm{T}}\right)=\boldsymbol{\Gamma}_1\mathbf{P}_{k|k}\boldsymbol{\Gamma}_1^{\mathrm{T}}+\boldsymbol{\Gamma}_2\mathbf{R}_k\boldsymbol{\Gamma}_2^{\mathrm{T}}+\Delta t^2\mathbf{Q}_k \tag{19}$$

As known in the measurement update equations of the classical KF, the posteriori state estimate is found as a linear combination of its *priori* state estimate and a weighted difference between the actual measurements and the corresponding predictions. Therefore, based on the revised observation equation as shown in Eq. (11), the posteriori state estimate $\hat{\mathbf{Z}}_{k+1|k+1}$ in this study can be can be calculated as

$$\hat{\mathbf{Z}}_{k+1|k+1}=\hat{\mathbf{Z}}_{k+1|k}+\mathbf{G}_{k+1}\left[\boldsymbol{\Phi}\mathbf{y}_{k+1}-\boldsymbol{\Phi}\mathbf{h}(\hat{\mathbf{Z}}_{k+1|k})\right] \tag{20}$$

where $\mathbf{G}_{k+1}$ is the KF gain matrix at time $t = (k+1)\times\Delta t$. Similarly, taking difference between Eqs. (5) and (20) leads to

$$\begin{aligned}\boldsymbol{\varepsilon}_{k+1|k+1}&=\mathbf{Z}_{k+1}-\hat{\mathbf{Z}}_{k+1|k+1}\\&=\left(\mathbf{I}-\mathbf{G}_{k+1}\boldsymbol{\Phi}\mathbf{H}_{k+1|k}\right)\boldsymbol{\varepsilon}_{k+1|k}-\mathbf{G}_{k+1}\boldsymbol{\Phi}\mathbf{v}_{k+1}\end{aligned} \tag{21}$$

where $\mathbf{H}_{k+1|k}$ can be determined using Eq. (16) while $\mathbf{Z}_k=\hat{\mathbf{Z}}_{k+1|k}$.

Then, the posteriori estimate error covariance matrix can be computed as

$$\begin{aligned}\mathbf{P}_{k+1|k+1}&=\left(\mathbf{I}-\mathbf{G}_{k+1}\boldsymbol{\Phi}\mathbf{H}_{k+1|k}\right)\mathbf{P}_{k+1|k}\left(\mathbf{I}-\mathbf{G}_{k+1}\boldsymbol{\Phi}\mathbf{H}_{k+1|k}\right)^{\mathrm{T}}\\&\quad+\mathbf{G}_{k+1}\boldsymbol{\Phi}\mathbf{R}_{k+1}\boldsymbol{\Phi}^{\mathrm{T}}\mathbf{G}_{k+1}^{\mathrm{T}}\end{aligned} \tag{22}$$

Based on the principle of KF technique, the optimality criterion used for determining gain matrix $\mathbf{G}_{k+1}$ is equivalent to minimizing the trace of the posteriori estimate error covariance matrix $\mathbf{P}_{k+1|k+1}$. Therefore, the gain matrix can be calculated by setting the partial derivative of $\mathrm{tr}(\mathbf{P}_{k+1|k+1})$ with respect to $\mathbf{G}_{k+1}$ to zero

$$\begin{aligned}\frac{\partial \mathrm{tr}(\mathbf{P}_{k+1|k+1})}{\partial \mathbf{G}_{k+1}}&=2\mathbf{G}_{k+1}\boldsymbol{\Phi}\left(\mathbf{H}_{k+1|k}\mathbf{P}_{k+1|k}\mathbf{H}_{k+1|k}^{\mathrm{T}}+\mathbf{R}_{k+1}\right)\boldsymbol{\Phi}^{\mathrm{T}}\\&\quad-2\mathbf{P}_{k+1|k}\mathbf{H}_{k+1|k}^{\mathrm{T}}\boldsymbol{\Phi}^{\mathrm{T}}=0\end{aligned} \tag{23}$$

in which $\mathrm{tr}(\cdot)$ denotes the trace operator. Then, the gain matrix can be found as

$$\mathbf{G}_{k+1}=\mathbf{P}_{k+1|k}\mathbf{H}_{k+1|k}^{\mathrm{T}}\boldsymbol{\Phi}^{\mathrm{T}}\left[\boldsymbol{\Phi}\left(\mathbf{H}_{k+1|k}\mathbf{P}_{k+1|k}\mathbf{H}_{k+1|k}^{\mathrm{T}}+\mathbf{R}_{k+1}\right)\boldsymbol{\Phi}^{\mathrm{T}}\right]^{-1} \tag{24}$$

On the basis of the posteriori state estimate $\hat{\mathbf{Z}}_{k+1|k+1}$ shown in Eq. (20), the unknown inputs at time $t = (k+1)\times\Delta t$ can be identified according to Eq. (9) as follows

$$\hat{\mathbf{f}}_{k+1}^{u}=\left(\mathbf{D}^{\mathrm{T}}\mathbf{D}\right)^{-1}\mathbf{D}^{\mathrm{T}}\left[\mathbf{h}(\hat{\mathbf{Z}}_{k+1|k+1})-\mathbf{y}_{k+1}\right] \tag{25}$$

As compared with Liu *et al.* (2016), it can be seen from Eq. (25) that the unknown input is identified on the basis of the posteriori state estimate $\hat{\mathbf{Z}}_{k+1|k+1}$ rather than the priori state estimate $\hat{\mathbf{Z}}_{k+1|k}$. As defined before, $\hat{\mathbf{Z}}_{k+1|k+1}$ is the estimate of $\mathbf{Z}_{k+1}$ at time $t = (k+1)\times\Delta t$. Thus, the usage of $\hat{\mathbf{Z}}_{k+1|k+1}$ for input identification should be more reasonable.

The flowchart of the proposed approach for joint estimation is plotted in Fig. 1. It can be found that the proposed approach has a similar frame of classical KF, including time update equations as shown in Eqs. (12) and (19) as well as measurement update equations as shown in Eqs. (20), (22) and (24). Also, the unknown excitations can be simultaneously identified according to Eq. (25). Moreover, the proposed approach can be used to handle both linear and nonlinear cases. The effectiveness and robustness of the proposed approach will be investigated in the following sections through some numerical examples and shaking table tests.

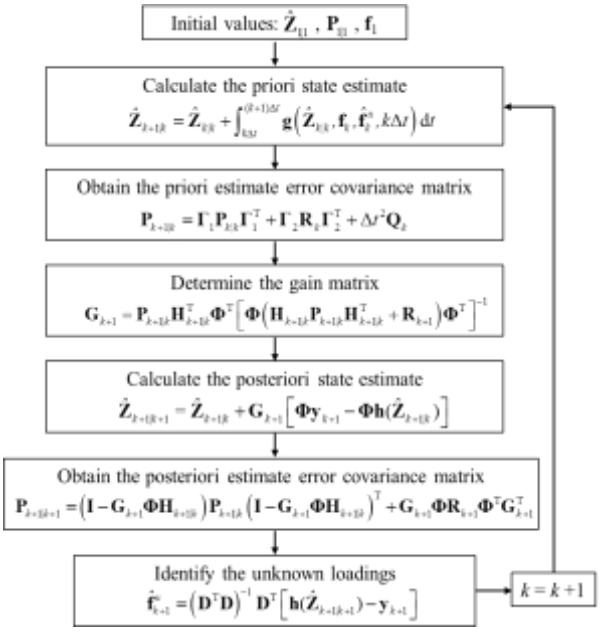

Fig. 1 Flowchart of the proposed approach

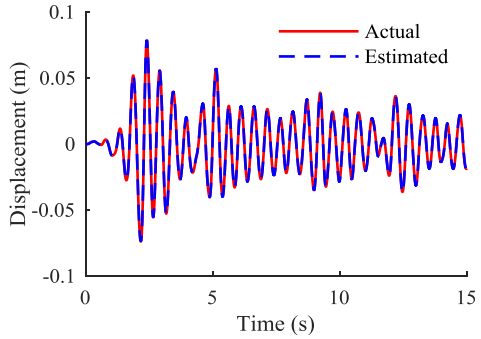

(a) Displacement of the top floor

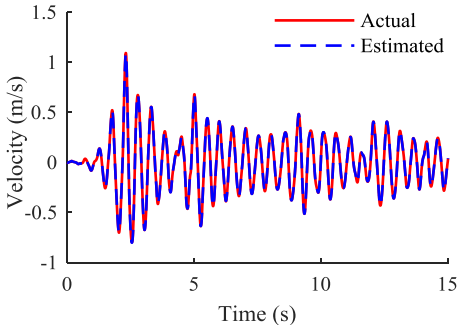

(b) Velocity of the top floor

Fig. 2 Comparison of structural responses of shear building structure

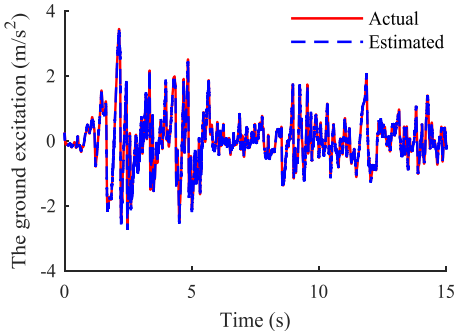

(a) The entire time series

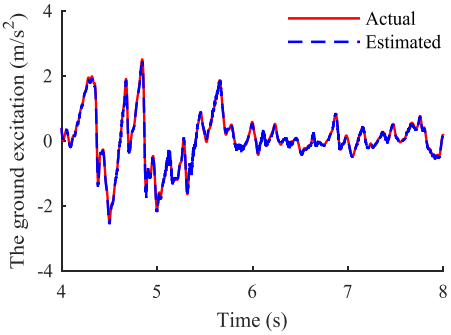

(b) Time segment from 4 s to 8 s

Fig. 3 Comparison of ground acceleration applied to shear structure

3. Numerical Investigation

In this section, several numerical examples including a five-story shear building, a simply supported beam and three types of nonlinear hysteretic structures are considered. The loadings used in these numerical examples are all assumed to be unknown. All the measured signals are simulated by the theoretically computed quantities superimposed with the corresponding noise process with 5% noise-to-signal ratio. Only limited acceleration responses are observed for the joint estimation. More details are given below.

3.1 Five-story shear building model

A five-story shear building is first employed for verifying the effectiveness of the proposed approach. The parameters of this model are given as m_i = 80 kg and k_i = 1.5×10^5 N/m (i = 1,…, 5). The Rayleigh damping assumption with the proportional coefficient of α = 0.5508 for mass matrix and β = 0.0012 for stiffness matrix is adopted for the construction of damping matrix. The structure is subject to the El-Centro earthquake with a peak ground acceleration (PGA) of 0.34 g, and the corresponding responses are calculated by state-space method with the time interval of 0.001 s. Herein, the acceleration responses of the 1st, 2nd and 4th floor are assumed to be measured for the joint estimation. As mentioned before, the response measurements are contaminated by 5% noise. The measurement noise and process noise covariance matrices are set to $\mathbf{R} = \mathbf{I}$ and $\mathbf{Q} = 10^{-4}\times\mathbf{I}$, respectively, where $\mathbf{I}$ is identity matrix with appropriate dimension.

Based on the proposed approach, the unmeasured structural responses, such as the displacement and velocity, can be estimated. Since the magnitudes of displacement, velocity, and in particular, the loadings are of different orders, a normalized root mean square error (NRMSE) defined in Eq. (26) is used as a measure of deviation between the actual and estimated values. The NRMSE results of the shear building are shown in Table 1.

Table 1 NRMSE results for shear building

Estimated quantities	NRMSE ($\times10^{-3}$)	Estimated quantities	NRMSE ($\times10^{-3}$)
x_1	1.44	v_1	0.15
x_2	1.37	v_2	0.11
x_3	1.34	v_3	0.88
x_4	1.33	v_4	0.54
x_5	1.36	v_5	0.13
$f_{seismic}$	7.00	-	-

* x_i and v_i denote displacement and velocity of the i-th floor, respectively

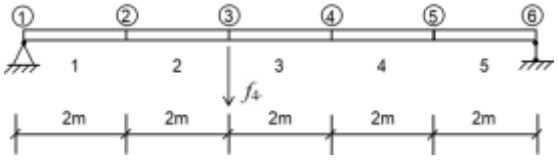

Fig. 4 Schematic diagram of a simply supported beam

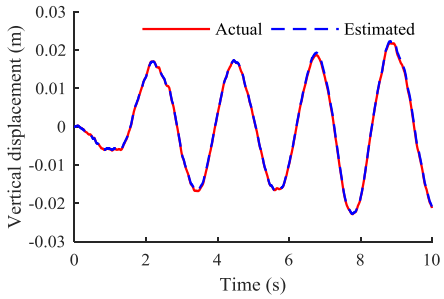

(a) Vertical displacement of node 3

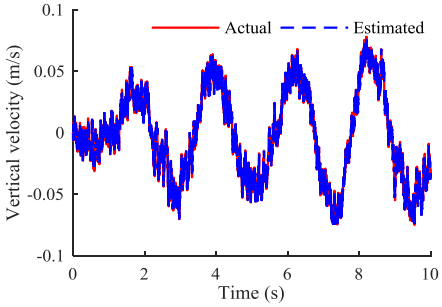

(b) Vertical velocity of node 3

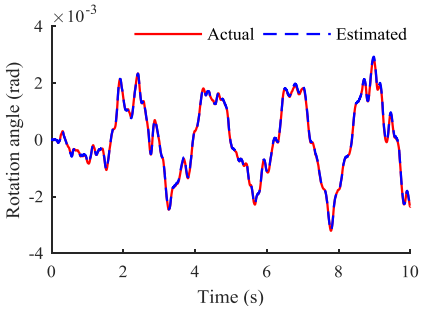

(c) Rotational displacement of node 3

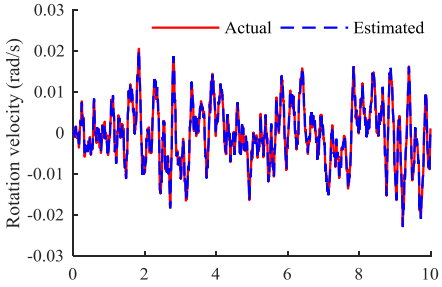

(d) Rotational velocity of node 3

Fig. 5 Comparison of structural responses of node 3

$$\mathrm{NRMSE} = \frac{1}{A}\sqrt{\frac{1}{np}\sum_{i=1}^{np}\left(\xi_i^{est} - \xi_i^{act}\right)^2} \tag{26}$$

in which A denotes the amplitude of the signal; np is the number of sampling points; ξ_i^{est} and ξ_i^{act} are the estimated and actual value of the i-th sample, respectively.

For ease and clarity of comparison, the time histories of the estimated structural states are also given in Fig. 2 as dashed curves, whereas the corresponding actual ones are plotted by solid curves. Due to the limitation of paper length, only the displacement and velocity responses of the top floor are given in Fig. 2 as an example. It can be seen from Fig. 2 that the estimated structural states have a good agreement with the actual ones. Similar results can be found for the remaining floors.

Besides the estimation of structural states, the unknown seismic loading applied to the building can be identified as well. The NRMSE of the identified input is also calculated and shown in Table 1. It can be found that values of NRMSE for the estimated structural states and unknown input are small. The comparison of time series of the identified input with the actual one is given in Fig. 3. For clarity of comparison, the time segment from 4 s to 8 s is also plotted in Fig. 3. It's obvious that the identified loading matches the actual one very well.

3.2 A simply supported beam

It is known the rotational response, such as the response of rotational angle, can be used for the assessment of structural safety and functionality. However, the direct measurement of rotational response is a challenging task. Therefore, the methods that can be used for the estimation of rotational responses would be another choice to gain rotational information.

In this example, a simply supported beam with identical cross section, as shown in Fig. 4, is used as an example for demonstrating the accuracy of the proposed approach for the estimation of rotational responses. The beam is divided into five elements with equal length. Each element has two nodes, and two DOFs are introduced for each node in the vertical and rotational direction. Notably, due to the constraints at nodes 1 and 6, only rotational DOF is involved in these two nodes. The parameters of beam are described as follow: elastic modulus E = 2 GPa, structural density ρ = 7850 kg/m^3 and area of cross section A = 0.04m^2. The Rayleigh damping assumption with the proportional coefficients of α = 0.1350 and β = 0.0043 is adopted, providing structural damping ratios $\zeta_1 = \zeta_2$ = 3%.

An unknown random excitation is applied to the beam in the vertical direction at node 3. As mentioned before, it would be difficult to directly measure dynamic responses of

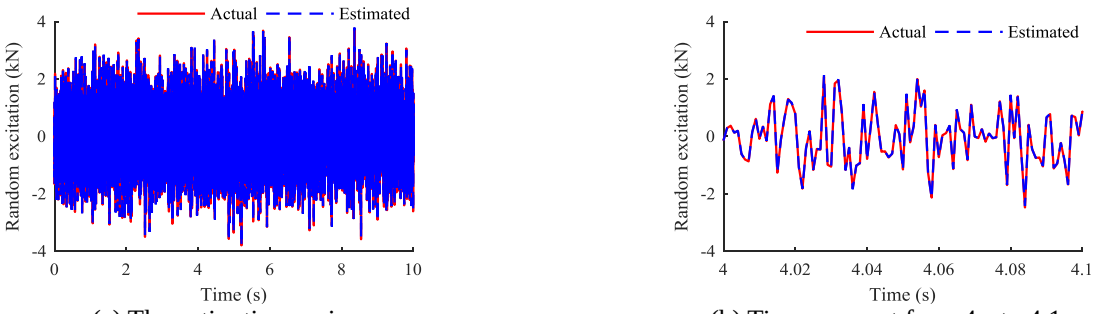

(a) The entire time series (b) Time segment from 4 s to 4.1 s

Fig. 6 Comparison of random force applied to simply supported beam

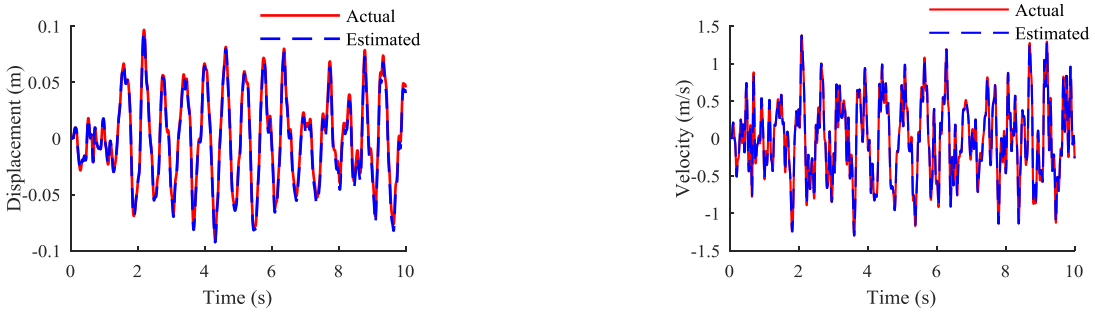

(a) Displacement of the top floor (b) Velocity of the top floor

Fig. 7 Comparison of structural responses of nonlinear system with Bingham model

rotational angles. Therefore, the rotational responses are unknown herein and only the acceleration responses in the vertical direction of nodes 2~5 are observed. Based on the proposed approach, the unmeasured structural responses and unknown input are estimated at the same time. The results of NRMSE are listed in Table 2. Taking node 3 as an example, the time histories of the estimated responses in the vertical and rotational direction are compared with their theoretical ones as shown in Fig. 5. Fig. 6 gives the comparison of the identified loading with the real one. Results shown in Table 2 and Figs. 5 and 6 indicate the proposed approach is feasible and reliable.

Table 2 NRMSE results for the simply supported beam

Estimated quantities	NRMSE ($\times 10^{-2}$)	Estimated quantities	NRMSE ($\times 10^{-2}$)
$x_{r,1}$	0.57	$v_{r,1}$	0.52
$x_{r,2}$	0.60	$v_{r,2}$	0.59
$x_{r,3}$	0.43	$v_{r,3}$	0.68
$x_{r,4}$	0.65	$v_{r,4}$	0.42
$x_{r,5}$	0.57	$v_{r,5}$	1.02
$x_{r,6}$	0.54	$v_{r,6}$	0.56
$x_{v,2}$	0.59	$v_{v,2}$	0.21
$x_{v,3}$	0.61	$v_{v,3}$	0.36
$x_{v,4}$	0.57	$v_{v,4}$	0.34
$x_{v,5}$	0.55	$v_{v,5}$	0.30
f_{random}	0.19	--	--

* $x_{r,i}$ and $v_{r,i}$ are displacement and velocity of the i-th node in the rotational direction, respectively; $x_{v,i}$ and $v_{v,i}$ are displacement and velocity of the i-th node in the vertical direction, respectively

3.3 Nonlinear hysteretic structure with Bingham model

To investigate the performance of the proposed approach for the estimation of nonlinear system, an eight-story shear-type building with a Bingham model on the 5th floor is employed. The values of mass and stiffness of the structure are set to be 80 kg and 2.6×10^5 N/m for each floor, respectively. The Rayleigh damping model with $\alpha = 0.4721$ and $\beta = 0.0014$ is used.

The nonlinear restoring force (NRF) generated by the Bingham model can be given by

$$R_f^{Bingham} = f_c \mathrm{sgn}(\Delta\dot{x}_i) + c_b \Delta\dot{x}_i + f_b \tag{27}$$

where f_c, c_b and f_b are the coefficients used for the description of the characteristics of Bingham model; $\Delta\dot{x}_i$ is the relative velocity between the i-th and (i-1)-th floor. Here, the parameters of Bingham model are set to be f_c =25 N, c_b =800 N·s/m, and f_b = −80 N.

In this example, a random excitation is applied to the 4th floor of building and the structural responses are calculated by Runge-Kutta method. The acceleration responses at the 1st, 2nd, 4th and 8th floor are assumed to be measured with the sampling frequency of 1000 Hz. Similarly, 5% noise level is considered.

Based on the proposed approach, joint estimation of the structural states and unknown input is conducted. The NRMSE results are listed in Table 3. It can be observed that the values of NRMSE for structural states and external excitation are small. Moreover, the time series of the estimated displacement and velocity responses of the top floor are compared with their actual ones in Fig. 7 as an

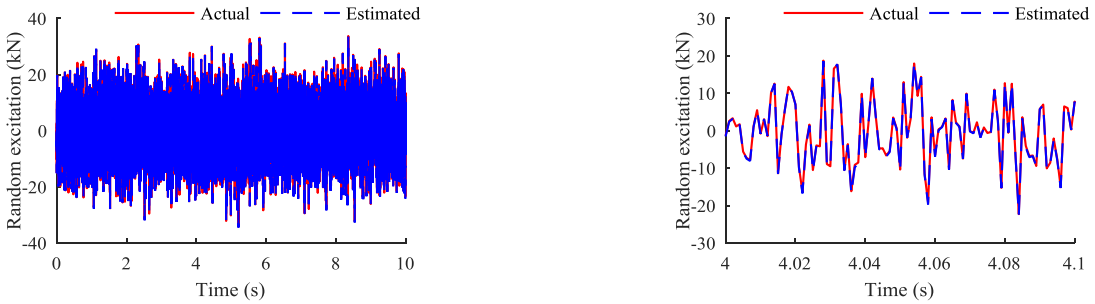

(a) The entire time series (b) Time segment from 4 s to 4.1 s

Fig. 8 Comparison of random force applied to the nonlinear structure with Bingham model

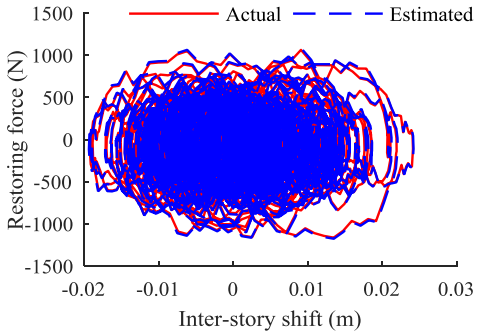

Fig. 9 Comparison of NRF provided by Bingham model

Table 3 NRMSE results for nonlinear hysteretic structure with Bingham model

Estimated quantities	NRMSE ($\times 10^{-2}$)	Estimated quantities	NRMSE ($\times 10^{-3}$)
x_1	1.77	v_1	0.98
x_2	2.22	v_2	1.15
x_3	2.64	v_3	1.43
x_4	3.11	v_4	2.62
x_5	2.68	v_5	1.65
x_6	2.42	v_6	1.13
x_7	2.14	v_7	1.11
x_8	1.97	v_8	0.50
f_{random}	0.41	--	--

example. The comparison of the identified excitation with the actual one is given in Fig. 8 Obviously, the proposed approach can satisfactorily estimate the structural responses of nonlinear system and the unknown input applied to it. Based on the estimated state vector, the NRF generated by Bingham model can be evaluated as well (see Fig. 9). Apparently, the estimated NRF is quite close to the real one which implies the proposed approach provides a potential way for the estimation of nonlinear characteristics.

3.4 Nonlinear hysteretic structure with Dahl model

To further investigate the performance of the proposed approach for different nonlinear system, an eight-story shear-frame structure with a Dahl model on the 1st floor is considered herein. The mass and stiffness parameters of the building structure are 300 kg and 1.4×10^5 N/m for each floor, respectively. The Rayleigh damping assumption with $\alpha = 0.1789$ and $\beta = 0.0038$ is adopted.

The nonlinear restoring force (NRF) provided by Dahl model in this example can be expressed as

$$R_f^{Dahl} = k_d \Delta x_i + c_d \Delta \dot{x}_i + f_d z + f_0 \tag{28}$$

where k_d, c_d, f_d and f_0 are the parameters describing the properties of Dahl model; Δx_i and $\Delta \dot{x}_i$ are the relative displacement and velocity between the i-th and (i-1)-th floor, respectively; z is a dimensionless coefficient as

$$\dot{z} = \sigma \cdot \Delta \dot{x}_i \left[1 - z \cdot \mathrm{sgn}(\Delta \dot{x}_i)\right] \tag{29}$$

in which σ is the coefficient controlling the shape of hysteresis loop, and sgn(·) denotes signum function. Here, the parameters of Dahl model are set to k_d = 30 N/m, c_d = 150 N·s/m, f_d = 400 N, f_0 = 0 N and σ = 1500 s/m.

The El-Centro earthquake with a PGA of 0.34g is applied to the building structure, and the nonlinear structural responses are obtained by means of Runge-Kutta method with the time interval of 0.001 s. The acceleration responses at the 2nd, 3th, 6th and 8th floor are assumed to be known, and the level of 5% noise is considered. Herein, the unknown quantities to be estimated include the state vector $\mathbf{Z} = \left[x_1, ..., x_8, \dot{x}_1, ..., \dot{x}_8, z\right]^{\mathrm{T}}$ and the unmeasured ground motion.

On the basis of the proposed approach, the estimation of the structural states and the unknown input are simultaneously conducted. Their NRMSE results are given in Table 4. Obviously, the values of NRMSE for both structural states and ground acceleration are small which means the results of the joint estimation by the proposed approach are reliable. Similarly, the comparison of time series of the estimated displacement and velocity responses of the top floor with their theoretical ones is shown in Fig. 10 as an example. Fig. 11 gives the comparison of the identified ground acceleration with the actual one. From Figs. 10 and 11, it can also be confirmed that the proposed approach is capable of estimating nonlinear structural responses and unknown input with acceptable accuracy.

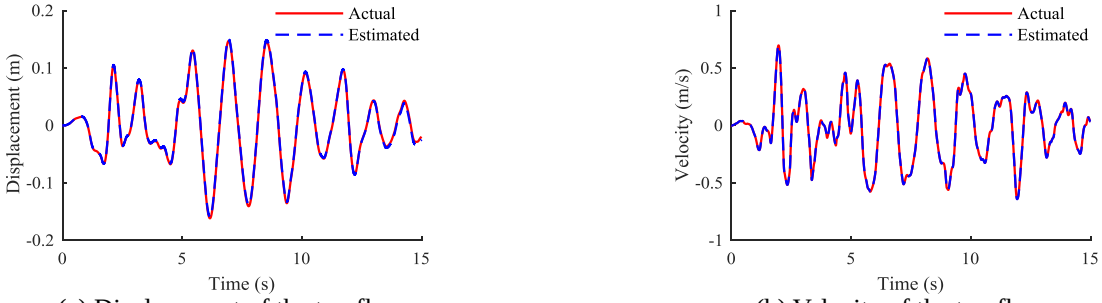

(a) Displacement of the top floor (b) Velocity of the top floor

Fig. 10 Comparison of structural responses of nonlinear system with Dahl model

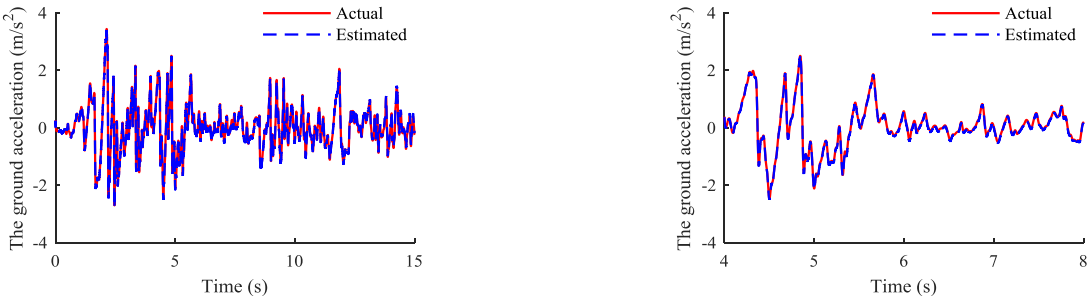

(a) The entire time series (b) Time segment from 4 s to 4.1

Fig. 11 Comparison of random force applied to the nonlinear structure with Dahl model

Table 4 NRMSE results for nonlinear hysteretic structure with Dahl model

Estimated quantities	NRMSE ($\times 10^{-3}$)	Estimated quantities	NRMSE ($\times 10^{-3}$)
x_1	9.60	v_1	1.17
x_2	9.14	v_2	0.72
x_3	8.77	v_3	0.74
x_4	8.19	v_4	0.84
x_5	7.76	v_5	0.86
x_6	7.44	v_6	0.93
x_7	7.21	v_7	0.87
x_8	7.09	v_8	0.79
$f_{seismic}$	5.01	--	--

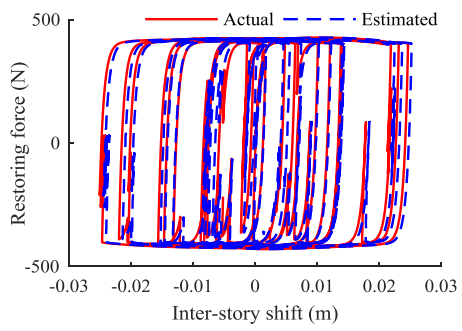

Fig. 12 Comparison of NRF provided by Dahl model

Moreover, on the basis of the estimated state vector, the NRF provided by Dahl model can also be evaluated as plotted in Fig. 12. It is clear that the estimated NRF has a good agreement with the real one.

3.5 Nonlinear hysteretic structure with Bouc-Wen model

To consider the joint estimation of building structure with multiple nonlinearities, an eight-story shear-type building with Bouc-Wen model on each floor is considered in this numerical example. The equation of motion of such nonlinear structure under earthquake excitation can be written as

$$\mathbf{M}\ddot{\mathbf{x}}(t)+\mathbf{C}\dot{\mathbf{x}}(t)+\mathbf{K}\mathbf{z}'(t)=-\mathbf{M}\mathbf{1}\ddot{x}_g(t) \tag{30}$$

where $\mathbf{z}'(t)$ is hysteretic component given as

$$\dot{z}_i'=\Delta\dot{x}_i-\eta_i\left|\Delta\dot{x}_i\right|\left|z_i'\right|^{\mu_i-1}z_i'-\gamma_i(\Delta\dot{x}_i)\left|z_i'\right|^{\mu_i} \tag{31}$$

in which η_i, μ_i and γ_i are the hysteretic parameters of Bouc-Wen model on the i-th floor. Here, the following values are employed: m_i = 125 kg, k_i = 20 kN/m, c_i = 100 N·s/m, η_i = 2000 s^{-2}, μ_i = 2 and γ_i =1000 s^{-2} (i = 1,…, 8). Instead of El-Centro earthquake, the seismic input considered in this example is Kobe earthquake with a PGA of 0.63 g. The nonlinear responses are computed by Runge-Kutta methods with the time interval of 0.001 s. The acceleration responses at the 1st, 3th, 5th, 7th and 8th, floor are considered for joint estimation. In this example, the state vector to be estimated is $\mathbf{Z}=\left[x_1,...,x_8,\dot{x}_1,...,\dot{x}_8,z_1',...,z_8'\right]^T$.

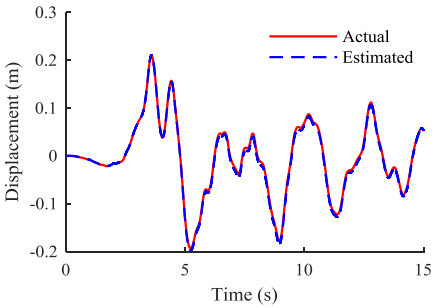

(a) Displacement of the top floor

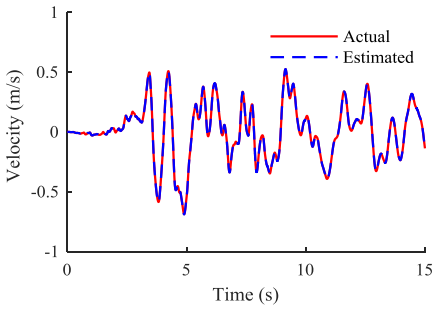

(b) Velocity of the top floor

Fig. 13 Comparison of structural responses of nonlinear system with Bouc-wen model

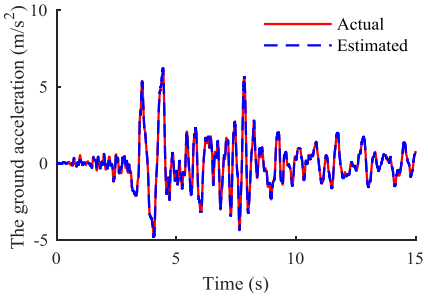

(a) The entire time series

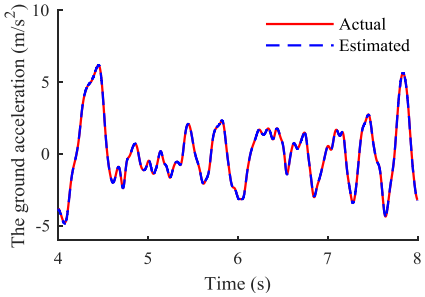

(b) Time segment from 4 s to 8 s

Fig. 14 Comparison of random force applied to the nonlinear structure with Bouc-wen model

Table 5 NRMSE results for nonlinear hysteretic structure with Bouc-Wen model

Estimated quantities	NRMSE ($\times 10^{-2}$)	Estimated quantities	NRMSE ($\times 10^{-2}$)
x_1	0.50	v_1	0.09
x_2	1.67	v_2	0.34
x_3	1.31	v_3	0.12
x_4	1.19	v_4	0.39
x_5	0.55	v_5	0.04
x_6	0.87	v_6	0.33
x_7	0.99	v_7	0.13
x_8	1.04	v_8	0.07
$f_{seismic}$	0.17	--	--

The results of NRMSE of the displacement, velocity and seismic input are shown in Table 5. Clearly, small values of NRMSE can be found in Table 5. The direct comparison of time series of the estimated displacement and velocity of the top floor is depicted in Fig. 13. Moreover, Fig. 14 gives the comparison of the identified ground acceleration with the actual one. The NRF provided by Bouc-Wen model can also be estimated as shown in Fig. 15. Again, it can be found from Figs. 13-15 that the differences between the estimated values and actual ones are very small.

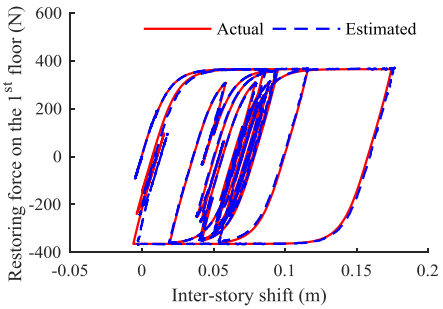

Fig. 15 Comparison of NRF provided by Bouc-Wen model

4. Experimental validation

The shaking table tests conducted on a five-story building model in the Dynamic Structural Laboratory of The Hong Kong Polytechnic University is employed herein to validate the robustness of the proposed approach for the joint estimation of a real structure. The building model as shown in Fig. 16 is designed as the height of 1750 mm and planar size of 850 mm × 500 mm. The rigid plates with the thickness of 16 mm are welded to four main columns with the cross section of 50 mm × 6mm and four smaller columns with the cross section of 10 mm × 6 mm. To increase the structural damping, five silicon oil dampers are designed and installed in the building structure. The lumped mass distribution of the building can be obtained basing on the weight measurement of each component, i.e., 67.43 kg,

61.65 kg, 56.54 kg, 62.82 kg and 59.66 kg for the 1st, 2nd, 3rd, 4th and 5th floor, respectively.

To determine the real values of structural stiffness, static tests as schematically shown in Fig. 17 are carried out. As the weight of the mass block increases, the displacement of each floor measured by the dial gauges increases. The tests are conducted three times, and the curves of average displacements of five floors (named as d1, d2, d3, d4, and d5) versus the loads in these tests are shown in Fig. 18. The structural stiffness of i-th floor k_i can be then calculated as

$$k_i = \frac{W}{d_i - d_{i-1}} \tag{32}$$

where W and d_i are the weight of mass block and the corresponding displacement of the i-th floor, respectively. Based on the measured results shown in Fig. 18, the values of stiffness are determined as 2.656×10^5 N/m, 2.576×10^5, N/m, 2.619×10^5 N/m, 2.639×10^5 N/m and 2.713×10^5 N/m for the 1st, 2nd, 3rd, 4th and 5th floor, respectively.

Moreover, by using a hammer to apply impact force to the top floor of the model, the analyses of structural dynamic properties are carried out on the basis of the measured acceleration and the corresponding frequency response functions.

Fig. 16 Five-story shear-type building structure

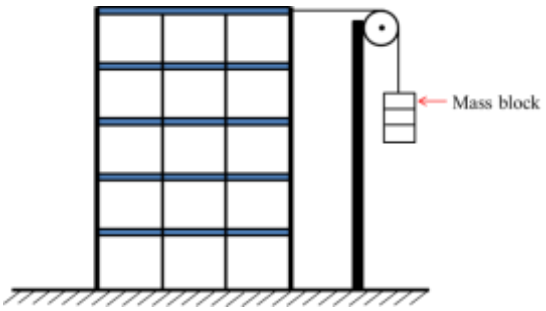

Fig. 17 Schematic diagram of static tests

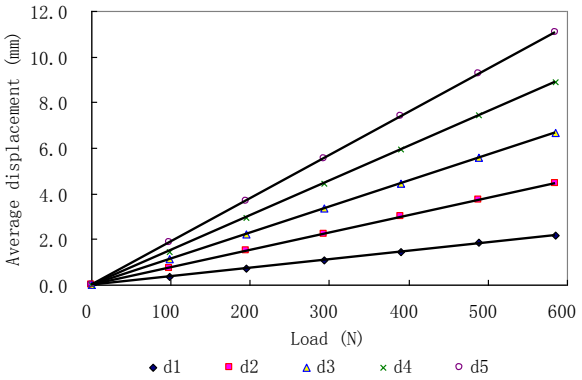

Fig. 18 Measured results in the static tests

The natural frequencies of the structure are found as 2.970 Hz, 8.658 Hz, 13.941 Hz, 17.948 Hz and 21.299 Hz. The first two damping ratios can be also found as 0.81 % and 1.01 %. The Rayleigh damping assumption is employed and the damping coefficients are determined as α = 0.1961 and $\beta = 3.051\times10^{-4}$.

Since the structural parameters including mass, stiffness and damping coefficients are obtained as described above, the shaking table tests used for the validation of the proposed approach are then conducted. The scaled Northridge earthquake with a PGA of 0.196g is considered as seismic input. The acceleration responses of the 1st, 2nd and 4th are measured for the joint estimation. For comparison, the seismic input and all of displacement responses are measured as well. The sampling frequency is set to 1000 Hz. To reduce the effect of measurement noise, a band-pass filter with the cut-off frequencies of 1 Hz and 30 Hz is used.

The quantities to be estimated include the structural states and unknown ground motion. By using the proposed approach for joint estimation, the results in terms of NRMSE are given in Table 6. The relatively small values of NRMSE can be found in Table 6 indicating the estimated results are reliable. The comparison of time series of the estimated displacement of the top floor with the measured one is shown in Fig. 19 as an example. It can be found from Fig. 19 that the estimated displacement is closed to the measured one. Similar results can be obtained for the remaining floors. Moreover, the identified seismic input is plotted in Fig. 20 as dashed line, whereas the corresponding measured one is shown as solid line. It is obvious that the identified excitation has a good agreement with the measured one.

Table 6 NRMSE results for five-story experimental structure

Estimated quantities	NRMSE	Estimated quantities	NRMSE
x_1	0.035	x_4	0.0251
x_2	0.0297	x_5	0.0241
x_3	0.0255	$f_{seismic}$	0.0122

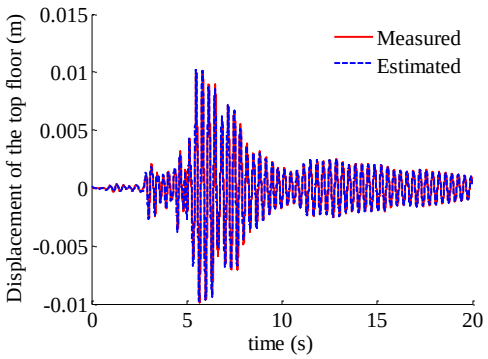

(a) The entire time series

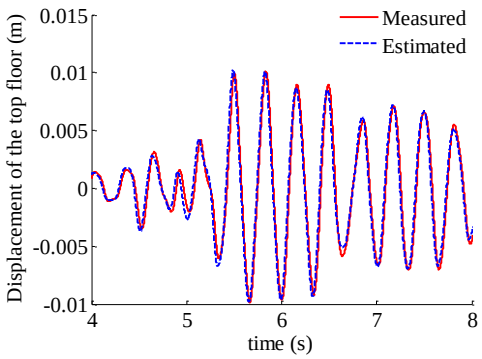

(b) Time segment from 4 s to 8 s

Fig. 19 Comparison of the displacement of the top floor in the experiment

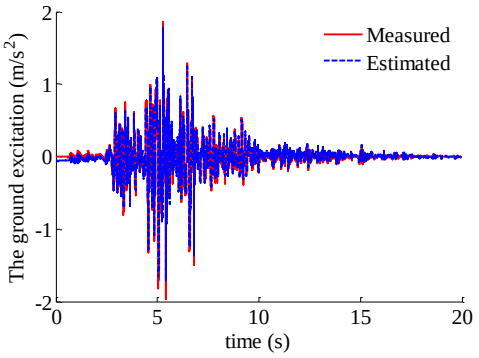

(a) The entire time series

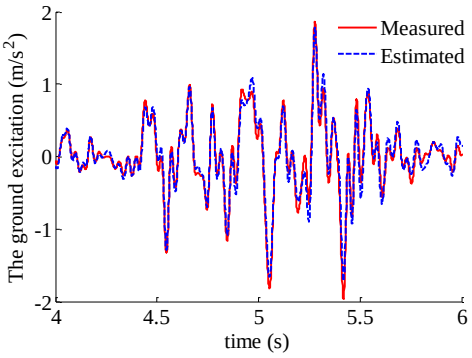

(b) Time segment from 4 s to 6 s

Fig. 20 Comparison of the seismic input used in the experiment

Notably, due to the measurements of velocity responses being not available in the tests, the comparison of the estimated velocity is not discussed herein. However, since the results of the estimated displacement and ground motion are acceptable, it can be concluded that the estimated velocity should be also reliable to some extent.

5. Conclusions

In this paper, an improved KF approach is proposed for joint estimation of structural states and unknown external excitations. By using a projection matrix, a revised observation equation with the unknown inputs being not explicitly presented is obtained. Based on the scheme of KF, analytical recursive solution of the proposed approach is derived, including the time update equations the measurement update equations. The unknown inputs are simultaneously identified by means of least squares estimation on the basis of the estimated structural states. With the consideration of nonlinear state space equation, the proposed approach can be used for joint estimation of both linear and nonlinear structural system with limited observations. The accuracy of the proposed approach is demonstrated via a five-story shear building, a simply supported beam, and three sorts of nonlinear hysteretic structures. The shaking tests of a five-story shear building structure are further conducted to validate the effectiveness and robustness of the proposed approach. Numerical and experimental results show that the proposed approach is capable of not only satisfactorily estimating structural states, but also identifying unknown loadings with acceptable accuracy for both linear and nonlinear systems.

Notably, as mentioned by Eftekhar Azam *et al.* (2015) and Liu *et al*. (2016), a drifted problem during identification procedure may occur. In this paper, the low-frequency drifts of estimation results are not happened mainly because of a high-pass filter being used prior to the state estimation. Based on the statement of Liu *et al.* (2016), further research will be conducted by data fusion of displacement and acceleration measurements to prevent the so-called drifts to realize real-time estimation.

Acknowledgements

The authors first would like to express their sincere thanks to Prof. You-Lin Xu and Mr. Sheng Zhan of The Hong Kong Polytechnic University for their strong supports and kind guidance for the shaking table tests. The authors also gratefully acknowledge the financial support from National Natural Science Foundation of China under project number of Grand No. 51708198 and No. 51468010. The support from National Natural Science Foundation of Hunan Province (No. 2018JJ3054) is also greatly appreciated.

References

Bernal, D. (2013), "Kalman filter damage detection in the presence of changing process and measurement noise", *Mech. Syst. Signal Pr.*, **39**(1-2), 361-371. DOI: 10.1016/j.ymssp.2013.02.012.

Ching, J. and Beck, J.L. (2007), "Real-time reliability estimation for serviceability limit states in structures with uncertain dynamic excitation and incomplete output data", *Probab. Eng. Mech.*, **22**(1), 50-62. DOI: 10.1016/j.probengmech.2006.05.006.

Eftekhar Azam, S., Ghisi, A. and Mariani, S. (2012a), "Parallelized sigma-point Kalman filtering for structural dynamics", *Comput. Struct.*, **92-93**, 193-205. DOI: 10.1016/j.compstruc.2011.11.004.

Eftekhar Azam, S., Bagherinia, M. and Mariani, S. (2012b), "Stochastic system identification via particle and sigma-point Kalman filtering", *Scientia Iranica*, **19**(4), 982-991. DOI: 10.1016/j.scient.2012.06.007.

Eftekhar Azam, S., Chatzi, E. and Papadimitriou, C. (2015a), "A dual Kalman filter approach for state estimation via output-only acceleration measurements", *Mech. Syst. Signal Pr.*, **60-61**, 866-886. DOI:10.1016/j.ymssp.2015.02.001.

Eftekhar Azam, S., Chatzi, E., Papadimitriou, C. and Smyth, A. (2015b), "Experimental validation of the Kalman-type filters for online and real-time state and input estimation", *J. Vib. Sound*, DOI: 10.1177/1077546315617672.

Eftekhar Azam, S., Mariani, S. and Attari, N.K.A. (2017), "Online damage detection via a synergy of proper orthogonal decomposition and recursive Bayesian filters", *Nonlinear Dynam.*, **89**(2), 1489-1511. DOI: 10.1007/s11071-017-3530-1.

Gao, F. and Lu, Y. (2006), "A Kalman-filter based time-domain analysis for structural damage diagnosis with noisy signals," *J. Sound Vib*., **297**(3-5), 916-930. DOI: 10.1016/j.jsv.2006.05.007.

Gillijns, S. and De Moor, B. (2007a), "Unbiased minimum-variance input and state estimation for linear discrete-time systems", *Automatica*, **43**, 111-116. DOI: 10.1016/j.automatica.2006.08.002.

Gillijns, S. and De Moor, B. (2007b), "Unbiased minimum-variance input and state estimation for linear discrete-time systems with direct feedthrough", *Automatica*, **43**, 934-937. DOI: 10.1016/j.automatica.2006.11.016.

He, J., Xu, Y.L., Zhang, C.D. and Zhang, X.H. (2015), "Optimum control system for earthquake-excited building structures with minimal number of actuators and sensors", *Smart Struct. Syst.*, **16**(6), 981-1002. DOI: 10.12989/sss.2015.16.6.981.

Hernandez, E.M. (2011), "A natural observer for optimal state estimation in second order linear structural systems", *Mech. Syst. Signal Pr.*, **25**(8), 2938-2947. DOI: 10.1016/j.ymssp.2011.06.003.

Hernandez, E.M., Bernal, B. and Caracoglia, L. (2013), "On-line monitoring of wind-induced stresses and fatigue damage in instrumented structures", *Struct. Control. Health Monit.*, **20**(10), 1291-1302. DOI: 10.1002/stc.1536.

Hsieh, C.S. (2009), "Extension of unbiased minimum-variance input and state estimation for systems with unknown inputs", *Automatica*, **45**(9), 2149-2153. DOI: 10.1016/j.automatica.2009.05.004.

Hu, R.P., Xu, Y.L., Lu, X., Zhang, C.D., Zhang, Q.L. and Ding, J.M. (2017), "Integrated multi-type sensor placement and response reconstruction method for high-rise buildings under unknown seismic loading", *Struct. Des. Tall Spec. Build.*, **27**(6), e1453, DOI: 10.1002/tal.1453.

Kim, D.W. and Park, C.S. (2017), "Application of Kalman filter for estimating a process disturbance in a building space", *Sustainability*, **9**, 1868. DOI: 10.3390/su9101868.

Lei, Y., Luo, S. and Su, Y. (2016), "Data fusion based improved Kalman filter with unknown inputs and without collocated acceleration measurements", *Smart Struct. Syst.*, **18**(3), 375-387. DOI: 10.12989/sss.2016.18.3.375.

Liu, L., Zhu, J., Su, Y. and Lei, Y. (2016), "Improved Kalman filter with unknown inputs based on data fusion of partial acceleration and displacement measurements", *Smart Struct. Syst.*, **17**(6), 903-915. DOI: 10.12989/sss.2016.17.6.903.

Lourens, E., Papadimitriou, C., Gillijns, S., Reynders, E., De Roeck, G. and Lombaert, G. (2012a), "Joint input-response estimation for structural systems based on reduced-order models and vibration data from a limited number of sensors," *Mech. Syst. Signal Pr.*, **29**, 310-327. DOI: 10.1016/j.ymssp.2012.01.011.

Lourens, E., Reynders, E., DeRoeck, G., Degrande, G. and Lombaert, G. (2012b), "An augmented Kalman filter for force identification in structural dynamics", *Mech. Syst. Signal Pr.*, **27**, 446-460. DOI: 10.1016/j.ymssp.2011.09.025.

Naets, F., Cuadrado, J. and Desmet, W. (2015), "Stable force identification in structural dynamics using Kalman filtering and dummy-measurements", *Mech. Syst. Signal Pr.*, **50-51**, 235-248. DOI: 10.1016/j.ymssp.2014.05.042.

Pan, S.W., Su, H.Y., Wang, H. and Chu, J. (2011), "The study of joint input and state estimation with Kalman filtering", *Trans. Inst. Meas. Control*, **33**(8), 901-918. DOI: 10.1177/0142331210361551.

Papadimitriou, C., Fritzen, C., Kraemer, P. and Ntotsios, E. (2011), "Fatigue predictions in entire body of metallic structures from a limited number of vibration sensors using Kalman filtering", *Struct. Control. Health Monit.*, **18**, 554-573. DOI: 10.1002/stc.395.

Ren, P. and Zhou, Z. (2017), "Strain estimation of truss structures based on augmented Kalman filtering and modal expansion", *Adv. Mech. Eng.*, **9**(11), 1-10. DOI: 10.1177/1687814017735788

Smyth, A. and Wu, M. (2007), "Multi-rate Kalman filtering for the data fusion of displacement and acceleration response measurements in dynamic system monitoring", *Mech. Syst. Signal Pr.*, **21**(2), 706-723. DOI: 10.1016/j.ymssp.2006.03.005.

Vicario, F., Phan, M.Q., Betti, R. and Longman, R.W. (2015), "Output-only observer/Kalman filter identification (O3KID)", *Struct. Control. Health Monit.*, **22**(5), 847-872. DOI: 10.1002/stc.1719.

Welch, G. and Bishop, G. (1995), "An Introduction to the Kalman Filter", Technical Report, University of North Carolina at Chapel Hill Chapel Hill, NC, USA, DOI: 10.1145/800233.807054.

Wu, A.L., Loh, C.H., Yang, J.N., Weng, J.H., Chen, C.H. and Ueng, T.S. (2009), "Input force identification: Application to soil-pile interaction", *Struct. Control Vib.. Control*, **16**, 223-240, DOI: 10.1002/stc.308.

Zhang, C.D. and Xu, Y.L. (2017), "Structural damage identification via response reconstruction under unknown excitation", *Struct. Control. Health Monit.*, **24**(8), e1953, DOI: 10.1002/stc.1953.

Zhi, L.H., Li, Q.S. and Fang, M.X. (2016), "Identification of wind loads and estimation of structural responses of super-tall buildings by an inverse method", *Comput.-Aided Civil Infrastruct. Eng.*, **31**, 966-982. DOI: 10.1111/mice.12241.

Zhi, L.H., Fang, M.X. and Li, Q.S. (2017), "Estimation of wind loads on a tall building by an inverse method", *Struct. Control. Health Monit.*, **24**, e1908, DOI: 10.1002/stc.198

Zhu, S., Zhang, X.H., Xu, Y.L. and Zhan, S. (2013), "Multi-type sensor placement for multi-scale response reconstruction", *Adv. Struct. Eng.*, **16**(10), 1779-1797. DOI: 10.1260/1369-4332.16.10.1779.

HJ